Journal of Sound and Vibration 603 (2025) 118989

Contents lists available at ScienceDirect

Journal of Sound and Vibration

journal homepage: www.elsevier.com/locate/jsvi

Body wave to surface wave conversion using tailored meta-structures

Rafael Fuentes-Domínguez [a], Richard J. Smith [a], Peng Jin [a], Marco Simonelli [b], Samuel Gibbon [b], Matt Clark [a,*]

[a] Optics and Photonics, Faculty of Engineering, University of Nottingham, University Park, Nottingham, NG7 2RD, UK
[b] Centre for Additive Manufacturing, Faculty of Engineering, University of Nottingham, University Park, Nottingham, NG8 1BB, UK

ARTICLE INFO

Keywords:
Acoustic waveguides
Mode conversion
Metamaterials

ABSTRACT

Elastic waves are important in many application areas. Their manipulation and coupling between different acoustic modes is important and presents a considerable challenge that offers to unlock the flexibility in wave transport required for efficient energy harvesting and vibration mitigation devices.

In this paper, we present a new class of metamaterial conversion devices consisting of arrays of "acoustic pipes" that can arbitrarily convert between different acoustic wavemodes. These pipes are used to match the modal patterns and phases between the two different elastic waves. The technique is fairly general and can be used to match any acoustic mode to any other acoustic mode provided an appropriate geometry can be formed.

Until recently the complexity of the geometries required has made the physical realisation of practical devices difficult because of the limitations of conventional fabrication processes but here we demonstrate practical devices made using additive manufacturing which can easily produce the complex topographies required for elastic waves around the MHz frequency region.

1. Introduction

Solids support many different wave modes. For instance, an isotropic, homogeneous, elastic medium supports two types of bulk waves: compressional, P, and shear, SV and SH, waves polarised vertically and horizontally that propagate with different wavespeeds C_p and C_s respectively with $C_p > C_s$ [1] and elastic half spaces also support surface waves, notably, the Rayleigh surface wave with a wavespeed C_R slower than both the bulk longitudinal and bulk shear wavemodes. Elastic plates also support an infinite number of highly dispersive Lamb modes [2]. This work extends emerging ideas explored in acoustic metamaterial arrays [3,4] and so-called rainbow trapping devices [3,5,6], ideas developed around optical holography [7], the properties of acoustic waveguides [8] and emerging manufacturing capability around additive manufacturing [9] to develop a novel way to manipulate wave propagation and create structures that couple energy between these various wave modes.

Taking advantage of this idea and the ability to manipulate the elastic wave speed, phase and amplitude with structures, it becomes possible to "rewire" the complex elastic wave amplitude to match both the incident and desired wavemodes and therefore to convert any incident wavefield into practically any other where it is physically possible to produce the required structure.

Elastic waves in solids, especially those confined to surfaces are important in a wide range of areas, for instance, surface acoustic wave microfluidic devices [10], acoustic microscopy [11,12] and of seismic wave and groundborne vibration propagation at the

* Corresponding author.
E-mail address: matt.clark@nottingham.ac.uk (M. Clark).

https://doi.org/10.1016/j.jsv.2025.118989
Received 1 March 2024; Received in revised form 15 November 2024; Accepted 27 January 2025
Available online 5 February 2025

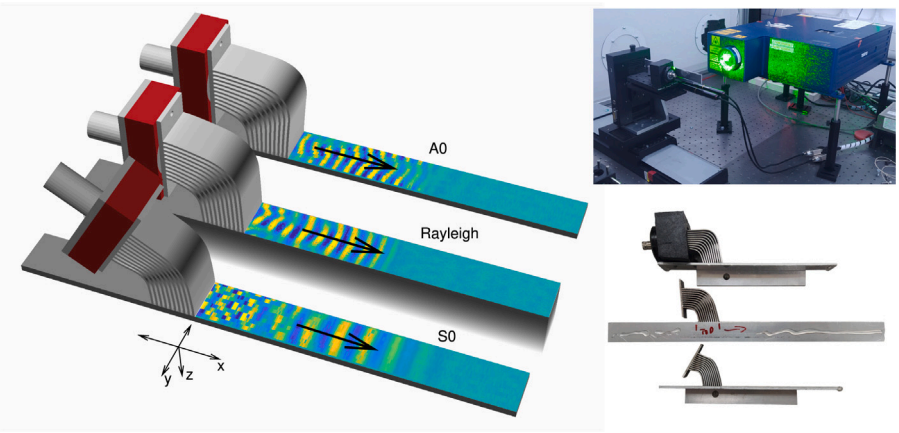

Fig. 1. Experimental results: (left) Schematic of the devices used overlaid with snapshots in time of scans of the surface displacement showing conversion of 500 kHz longitudinal waves at the transducer to A0 Lamb waves, Rayleigh waves and S0 Lamb waves on substrates (3 mm thick for Lamb waves, 20 mm thick for Rayleigh waves). The devices consist of an array of curved plates, 1 mm thick, which are bent so that the displacement arriving at the substrate surface is phase-matched to the relevant wavemode on the substrate. Each plate is separated by 1 mm at both the transducer and substrate ends and joins both the transducer and substrate ends at normal incidence. (right, top) Photo of the experimental configuration, with laser interferometer and sample mounted on scan stages with transducer mounted. (right bottom) Photos of devices mounted on substrates (top-bottom, A0 (with transducer), Rayleigh and S0 devices). Polymer beads to control reverberations can be seen at the ends of the A0 and S0 and sides of the Rayleigh wave devices (see Section 5).

large scale [13–15]. They are also potentially important for energy harvesting [16] by matching incident wave modes to those easily suited to piezoelectric devices [17,18]. As such the devices presented here and the general methodology should prove influential in the control of elastic wave energy for a wide range of applications. The methodology presented is not confined to elastic waves in solids and could be extended to acoustics, underwater acoustics and optics.

In this article we present experimental results demonstrating the conversion of body (longitudinal) waves into Rayleigh, and A_0 and S_0 Lamb modes. Furthermore, we present simulation results showing that a wide range of higher order modes can be efficiently coupled to (see Appendix A) and that, within limits, the body wave can be arbitrarily redirected.

The working principle of these devices requires matching one modal pattern and phase distribution with another modal pattern and phase distribution and then finding a structure that can reorganise the modal shape and match the phases. Essentially it requires routing the nodes of one mode to the nodes of another with the appropriate time or phase delays. In this vision it is possible to "re-wire" any mode into any other mode (or spatial distribution) of the same frequency provided it is possible to design and realise a structure to physically connect them with the required geometry and phase delays. In this paper we demonstrate this for longitudinal to surface/plate mode conversion but the technique is general provided the structure can be realised (albeit with some limitations for special cases).

In the context of the conversion between longitudinal surface/plate modes this is already possible through the use of elastic wedges [19] or inter-digitated structures [20] but these techniques lack the generality or flexibility of the technique demonstrated here as their geometries are restricted and there are a limited number of modes that they can excite. Furthermore, the geometry and material requirements of these existing techniques are highly restricted making them of limited value in many applications such as seismic/vibration control and energy harvesting. By contrast, the technique demonstrated here can potentially convert any mode into any other mode (caveats apply) propagating in any direction including between separate physical domains or between modes in the same domain. Thus it would be possible to convert between a surface mode and a bulk mode in the same substrate or to redirect surface modes into diving bulk modes away from the surface.

Since it is also possible to couple from one mode to the same mode, but with an arbitrary spatial or phase distribution it would also be possible to redirect or shape the wavefronts of the acoustic waves forming devices equivalent to acoustic mirrors or lenses.

2. Design paradigm

Consider two surfaces S_s and S_d representing the source and destination of the elastic waves, U_s and U_d, to be coupled. The complex amplitudes of the waves are U_{S_s} and U_{S_d} at S_s and S_d respectively (Fig. 2 (left)). These are to be connected by elastic waveguides (pipes), which must sample and couple to the source and destination on a spatial scale finer than the k-vectors of U_{S_s} and U_{S_d} resolved along S_s and S_d respectively. The pipes must also efficiently couple to the wavemodes of U_s and U_d at each end. In this study the source is a flat plane with a normally incident longitudinal wave and the destination is a flat plane with a surface wave propagating along it. In this case the pipes, acting as waveguides, consist of thin plates each supporting a quasi-longitudinal plate mode (S0 Lamb mode as the thickness $\to 0$ relative to the wavelength [8]) in order to couple the wavemodes in the source and destination together. In order to match the motion of the wavemodes in the source (longitudinal) and destination (surface wave) these pipes need to efficiently couple the wave motions of this quasi-longitudinal mode in the pipe to the mode in the source or

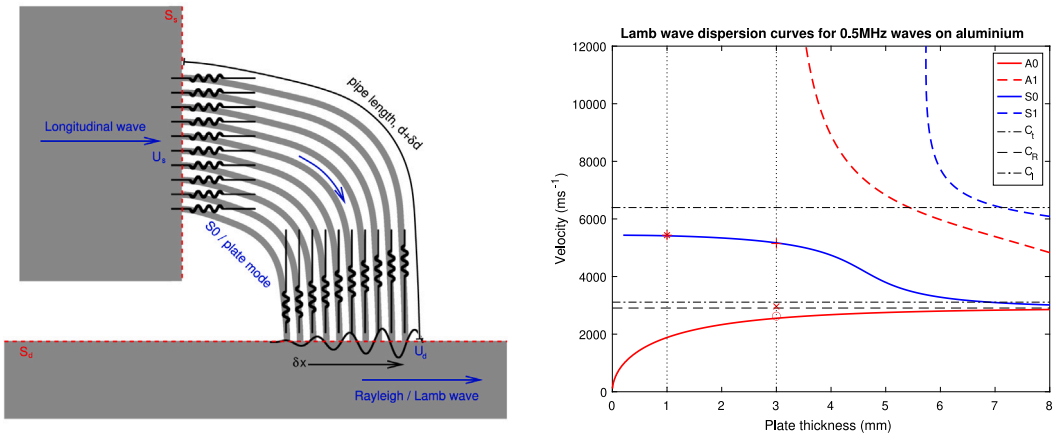

Fig. 2. (left) Schematic of the device and its mode of operation. The incident longitudinal wave enters the device and is divided amongst the "acoustic pipes" which act as waveguides. This device is designed to excite the S0 Lamb modes in the pipes and then match this to a variety of modes in the substrate. The pipes are "thin" and the S0 mode velocity is close to the plate velocity of the waveguide (marked with + on the dispersion curves, right). The length of the pipes is arrange to phase match with the desired travelling wave in the substrate. Maximum conversion efficiency between the original longitudinal and the pipe, and the pipe and the substrate was found to occur at normal incidence. Consequently geometry of the pipes must be arranged to join the surfaces at the required positions at normal incidence and have the pipe lengths required. There is no requirement for the pipes to join the substrate at any specific spacing. In this design, 1 mm thick plates with 1 mm spacing were used for all examples. (right) Lamb wave dispersion curves showing A0, A1, S0 and S1 velocities as a function of plate thickness for the 0.5 MHz excitation used in this paper. The vertical lines show the thicknesses of the "pipes" (1 mm) used in the device and the thickness of the substrate used in the Lamb mode excitation experiments (3 mm), the Rayleigh mode experiment used a 20 mm thick substrate. The horizontal lines show the non-dispersive shear, Rayleigh and longitudinal mode velocities. The markers ∘, ×, + show the measured velocities on the substrates for the various modes and the * marks the design point for the plates used for the acoustic pipes. The red annotation shows the surfaces and fields defined in the body text. (For interpretation of the references to colour in this figure legend, the reader is referred to the web version of this article.)

destination. In this case it can be achieved by joining the pipe to the surface at normal incidence (Fig. 2). The k-vector of the waves resolved along the surface of both the source and destination must be adequately sampled by the pipes meaning that pipe thickness must be smaller than the wavelength of the wavemode resolved along the surface. In the case presented here, the wavevector of the source wave is effectively zero due to the normal incidence of the longitudinal wave and the k-vector of the surface waves on the substrate is determined by the modes' wavelength, which, in turn, is determined by the speed of the mode and the frequency. In this study $f = 0.5$ MHz and $C \sim 2500 - 6000$ ms^{-1} resulting in $k \sim 1200 - 500$ radians/m so acoustic pipes made of ~1 mm thick aluminium plates easily meet this sampling condition.

The modal patterns of both U_{S_s} and U_{S_d} along S_s and S_d have a constant complex amplitude. Across S_s this has a constant phase and across S_d it is a linearly varying phase along the direction of propagation given by $\phi_d = 2\pi\delta x/\lambda_d$, where δx is the distance along S_d in the direction of propagation and λ_d is the wavelength of U_{S_d} at S_d. In order to match the modes an equal phase needs to be gained along the pipes joining S_s and S_d. This can be obtained by varying the lengths of the pipes and the excess length of the pipes along x is given by $\delta d_{pipe} = \delta x C_{plate}/C_{pipe}$ (see Fig. 2). This could also be achieved by modulating the wavespeed along the pipe either by changing the pipes' effective elastic modulus (or density) or, in this case, by changing the pipes' plate thickness in order to change the speed of the S0 Lamb wave.

The design problem then reduces to finding a topology for the set of plates that have the appropriate lengths and distributions along S_s and S_d that are also normally incident to both surfaces. This was achieved with plates that were curved to match the position and direction at each surface and also to match the required length along the pipes to obtain the correct phase delay. These curves were made by using a cubic spline with 5 constraint points, two to define the position and direction at each end and a fifth placed mid way along the curve whose position was adjusted to obtain the correct length. Where this led to undesirable shapes from a manufacturing point of view (i.e. the plates became too close for manufacturing tolerances) the location and angle of S_d was optimised to result in a suitable structure for fabrication (Fig. 2) (see Section 4).

In order to create the pipe/waveguide there must be physical gaps between the waveguides, else the boundary conditions for the waveguide will cease to exist. The width of the gaps is not important for their operation so long as it is sufficient to prevent any contact or mechanical coupling between them. However, it is important for the fabrication of the devices that the gap has to be greater than the resolution of the fabrication process and in the devices presented here the gap has to also facilitate the removal of unused metal powder from between the pipes (see Section 4). In this case, a nominal minimum distance of 1 mm was chosen between the pipes for all designs where the pipes contact the surfaces S_s and S_d. However, the gap spacing was allowed to vary along pipe (between the source and destination surface). It was important to find a solution where the pipes remains separated and the gap did not violate the minimum separation required at any point along the pipe. In addition, the designs were kept compact and the position and angles chosen for the source and destination were set by practical considerations such as to facilitate the attachment of the transducers and give as clean line of sight to the substrate surface as possible for measurement and scanning. The devices for A0, Rayleigh and S0 conversion are shown in Fig. 1. It should also be noted that the spacing of the pipes at the surface

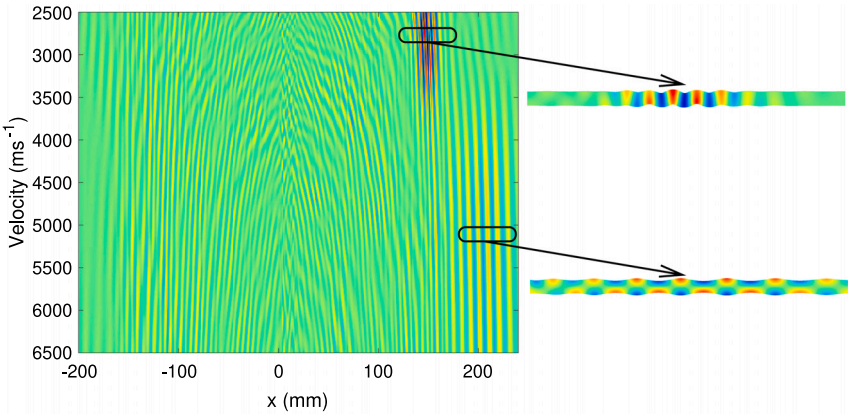

Fig. 3. Simulation of devices: (left) In this simulation the substrate is kept at 3 mm thick and the geometry of the device is changed to couple to different velocities. The target velocity is swept from 2500 to 6500 ms^{-1} along the y-axis. This is achieved by changing the pipe lengths to phase match with the desired velocity. The result of the simulation (in the form of the surface displacement) at a single moment in time (60 μs) is plotted along the x-axis. The presence of an excited wavemode is revealed as a waveform by the periodic oscillations to the left or right of $x = 0$ (where the device is placed). positive x-direction indicates the direction of propagation the device was designed for. In this plot, it can be observed that the excitation in the positive x-direction is significantly higher than the negative direction. At various target velocities it can be observed that different modes are preferentially excited when the phase of the plate mode matches the phase delay of the exciting waveguides. On this figure the A0 and S0 Lamb modes can be observed at velocities of 2750 and 5250 ms^{-1} respectively. Interpreting this plot is not trivial because the dispersion of the plate modes results in significant changes to the group velocity (see [2]), however, it is easy to confirm the correct modes by examining their modal patterns (right). The dispersion curves can be seen in Fig. 2. Extended simulations showing additional modes can be found in Appendix A. A discussion on the effect of the group velocity can be found in Appendix B.

is not required to be an integer number of wavelengths as for comb and interdigitated transducers [2,20] and can be any spacing so long as the fabrication design rules and sampling discussed above are met. This allows a wide range of design freedom and will also allow additional engineering of the structures to tailor other aspects of the devices, for instance, the frequency response and control of the bandwidth [21].

In the low and mid-band frequency regimes (see Section 2.1 below) the S0 mode in the pipe gives rise to a predominantly piston like displacement at the end of the pipe with uniform displacement amplitude across the pipe (see [2]). This can be considered as a piston excitation source with uniform phase across the width of the pipe. In order for the phase matching condition to be valid along the substrate, the width of the pipes at the point of contact with the substrate must be significantly less than the wavelength of the desired wave on the substrate. This can be thought of as analogous to the Nyquist sampling condition for the desired mode.

2.1. Frequency regime, bandwidth and size scale

The frequency operation of these devices can be divided into four regimes: low frequency, mid-band, mid-high frequency and high frequency.

The devices demonstrated here operate in the mid-band region which is characterised by having wavelengths smaller than the length of the pipes and larger than the thickness of the pipes. In this regime the S0 wave speed in the pipes is more or less constant and the S0 mode is the only mode that is excited (the A0 is not excited because of the symmetry of the system). As the S0 wave speed in this region tends to the plate mode velocity the wave speed in the pipe can be treated as dispersion free. In this regime it is easy to modulate the phase of the S0 mode at the end of the pipe by changing the length of the pipe so it is easy to phase match with the substrate wave modes.

In the low frequency regime, the S0 velocity becomes fixed at the plate mode velocity and is non-dispersive but the wavelength of the sound in the pipe becomes comparable or longer than the length of the pipe itself. Consequently it becomes impossible to effectively modulate the phase along the pipe by any appreciable amount because the propagation distance is too small. Therefore it is not possible to phase match with the substrate.

In the mid-high frequency regime the wavelength approaches or becomes smaller than the pipe thickness and the dispersion in the pipe becomes significant but the frequency remains below the higher order Lamb mode cut-off. In this regime it might still be possible to achieve phase matching with the substrate for narrow bandwidths but it might not be possible to ensure that the pipe thickness is less than the substrate wavelength (which is another condition required for efficient generation). However, in this regime it may be possible to modulate the thickness of the pipes to achieve a means of modulating the wave speed and therefore controlling the phase at the end of the pipe. This might also be used to achieve phase matching (without changing the length of the pipe).

In the high frequencies regime, above the S1 cutoff frequency, additional modes may be excited (eg S1 or S2) which will complicate the design and might excite additional modes in the substrate. In this case the design of the devices will become extremely challenging and it will become difficult to meet the sampling conditions for the wave on the substrate as discussed in the previous section.

2.1.1. Bandwidth

In the design regime (mid-frequency) these devices are dispersion free and broadband so long as they remain in the mid-frequency regime. For the devices/geometries presented here the frequency range of normal operation for the generation of non-dispersive wave modes such as the Rayleigh wave the bandwidth of the device is estimated as 0.2–3.0 MHz.

However, if the desired wave mode itself is dispersive these devices will be narrowband because the phase matching depends on the substrate's wave velocity. For the A0 and S0 Lamb mode devices the bandwidth is dominated by the dispersion of the substrate and estimated to be ±64 kHz and ±129 kHz respectively. In this case the bandwidth is determined by the total size of the region occupied by the acoustic pipes on the substrate surface. With fewer pipes, and a smaller region, the bandwidth might be increased, however, the mode and directional selectivity will be decreased. However, it might be possible to create extended bandwidth devices in these circumstances, without sacrificing selectivity, by balancing the dispersion of the acoustic pipes in the mid-high frequency regime with the dispersion in the substrate.

2.1.2. Size scale

In the design regime (mid-frequency) the size of the required structure can be estimated as several times the wavelength of the sound to be controlled. This allows the size to be estimated for different regimes, for instance: at 1 MHz for metals the approximate size is ~ 15 mm and for seismic waves (~10 Hz) in soft soils (C~ 150 ms^{-1} [22]) the required size is ~ 75m.

3. Simulation

The devices were simulated using Comsol Multiphysics [23] in 2D using the structural mechanics module. This was used to perform transient finite element analysis of time evolving displacement in the source (transducer) and destination (plate) substrates and in the acoustic pipes linking them. In the simulation results shown here (Fig. 3) the thickness of the destination substrate was kept constant (3 mm) and the length of the acoustic pipes was varied to phase match surface acoustic waves with velocities from 2500 ms^{-1} to 5500 ms^{-1}. The excitation was simulated by setting the surface displacement at the transducer to a 0.5 MHz sinusoidal signal with a Gaussian amplitude envelope resulting in an approximately 3 cycle sinusoidal excitation burst. A low reflection boundary condition was used at the ends of the substrates and a stress free surface boundary was used elsewhere. The structure was meshed for at least 10 elements per wavelength. The modes excited were recorded at a fixed point in time (60 μs) and the surface displacement along the surface of the substrate (x-axis) was plotted as a function of the thickness of the substrate (y-axis, see Fig. 3).

In Fig. 3 the presence of A0 and S0 modes can be seen corresponding to their phase velocities predicted by Lamb wave theory (see Fig. 2). Interpreting this figure is complex because of the highly dispersive phase and group velocities, however, the modes can be unambiguously identified from their modal patterns (Fig. 3) [2]. Additional analysis is available in the Appendix B.

This model confirms the ability of these devices to generate a variety of modes and to impart a strong directionality to the energy converted. The model has also been used to explore other thicknesses and confirms the ability of these devices to excite a wide range of modes including Rayleigh, A0, S0, A1, S1 and S2 modes (see Appendix A). A notable exception to this generality is in the vicinity of some non-propagating wavemodes such as the S1 (S_2^b) zero-group-velocity (ZGV) Lamb mode [2,24]. This exception arises from the strong coupling of the acoustic pipes to the substrate. This can be thought of as either the pipes perturbing the very precise conditions needed to create the ZGV modes or as the energy from these modes being strongly coupling straight back out along the waveguides. Either way, the excitation of these standing waves might be possible by more weakly coupling the waveguides to the substrate.

4. Design and fabrication of the devices

The devices were prepared for manufacture using openSCAD [25]. The curves for the acoustic pipes were computed in Matlab [26] / Octave [27], which was also used to prepare the openSCAD to lay out the structures. Matlab/Octave were also used to compute the velocities and dispersion properties of the wavemode used after [1,2]. The devices were then rendered using openSCAD to produce STL files for printing. Scale drawings of the devices are shown in Appendix C.

The parts were printed using a Renishaw AM400 selective laser melting additive manufacturing system from a standard additive manufacturing aluminium alloy (AlSi10Mg). This "prints" the parts by using a high power laser beam to selectively melt a bed of metal powder. Once each layer is written, a thin layer of powder is added and the next layer is written [28]. This alloy has a quoted elastic modulus of 75 ± 10 GPa and a density of 2.67 g/cm^3. The large error on the elastic modulus reflects the variation of the elasticity measurement with various build conditions and was used in the design and analysis of these devices without further measurement.

The parts were printed on their sides and removed from the build plate using electrical discharge machining (EDM) cutting. By printing on their side the need for any supporting structure was eliminated. The contact surfaces for application to the substrate and the transducer were then lightly ground using a 240 grit abrasive to prepare them for adhesion to the substrate.

The devices were attached to the substrate using cyanoacrylate adhesive ("superglue") and care was take to ensure the glue layer was as thin as possible and that the devices were carefully aligned with the axis of the substrate.

The transducers were attached to the devices using custom mounts printed in PLA plastic using a standard FDM 3d printer (Ultimaker). Standard ultrasonic couplant gel was used to coat the transducer and device surface prior to attachment and care was taken to eliminate bubbles and to ensure that the couplant did not dry out during measurements.

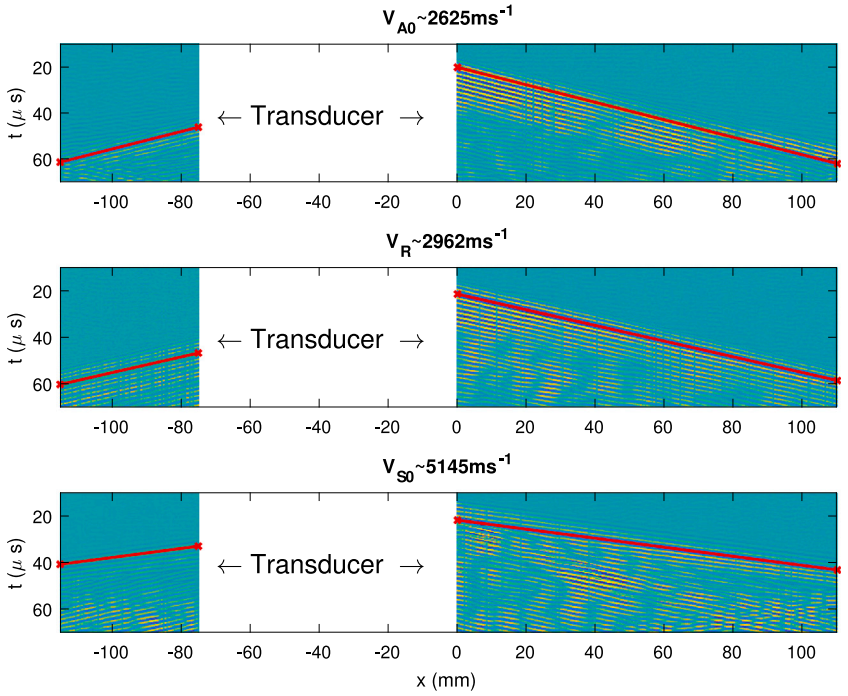

Fig. 4. Experimental b-scans for the three devices investigated. At positive values of the x-axis these show the A0, Rayleigh and S0 modes travelling in the design direction of the devices. The red lines show the gradient of the phase velocity that was used to experimentally determine the velocity for each mode. At negative value of the x-axis this shows the resulting waves behind the devices. The white region marked "transducer" is blocked from measurement by the device and transducer (see Fig. 1). The amplitudes at positive directions are > 3× those in the negative direction. Close examination of the A0 and S0 b-scans shows the effect of the dispersion on the group velocity which is slower and faster, respectively, than the phase velocity. This is absent for the Rayleigh mode which is non-dispersive. More details are shown in the Appendix B. (For interpretation of the references to colour in this figure legend, the reader is referred to the web version of this article.)

5. Experimental verification

To experimentally verify the concept three devices were fabricated and tailored to produce A0 Lamb waves, Rayleigh waves and S0 Lamb waves respectively. These were fabricated using 3D printed aluminium as previously described and glued to 3 mm, 20 mm and 3 mm thick substrates respectively. The designs were fabricated 20 mm wide to match the width of the substrates. This was slightly narrower than diameter of the active transducer element (25 mm) to ensure an even excitation of the waves. As the devices were not very wide compared with the design wavelengths some slight diffraction in the transverse direction might be expected. This may be apparent in the experimental results shown in Fig. 1, however, these effects may also be a result of slight apodization due to the circular transducer shape and, as can be observed in Fig. 1 the effects are minimal. Nevertheless the results presented in Fig. 4 are taken from the centre line along the substrate.

A plane longitudinal wave piezo-electric transducer was attached to the longitudinal wave end of the device and used to excite surface/plate waves in the substrates (see Fig. 1). The transducer was excited by a Ritec 400 pulser set to generate a 3 cycle, 0.5 MHz waveform with a 200 Hz repetition rate.

It was observed that the 0.5 MHz ultrasound signal would circumnavigate the entire sample several times taking over 10 ms to ring-down. To prevent the reverberating signals from ringing for too long soft polymer beads applied via a hot glue gun were attached to the ends of the substrates to acts as acoustic energy absorbers. These were effective in ensuring a more rapid ring down in under 2 ms so that no signal, above the noise, could be observed at the start of the next pulse (see photographs in Fig. 1).

The thin substrates for the A0 and S0 Lamb wave experiments were prepared by cutting strips from a 3 mm aluminium plate, which were then mounted to a carrier along one edge using cyanoacrylate adhesive so they could be easily mounted in the optical system. There is little evidence that this affected the measurements evident in any of the results. The Rayleigh wave substrate was prepared from aluminium bar and machined down to 20 mm thick. At 20 mm the substrate was sufficiently thick so that the A0 and

S0 Lamb modes could effectively hybridise and be considered as a pure Rayleigh wave over the experimental distances examined [2]. In this case, the distance to the first null on the top surface created by the beating of the A0 and S0 modes was estimated to be around 6 m, ∼20× the size of the experiment justifying treating this as a pure Rayleigh wave device. This is evident in Fig. 4 where no beating can be observed in the middle plot. This substrate was sufficiently thick that no additional mount was required.

The samples were mounted on scan stages (Physik Instrumente) which allowed them to be scanned over their entire surface with a nominal positional accuracy of 1 μm. The signals were detected with a Sound & Bright BossaNova adaptive photorefractive laser interferometer. This was set to measure absolute displacement so the amplitudes from each scan could be directly compared. The signals were captured using a LeCroy Waverunner 9254M oscilloscope and averaged 100 times. The longitudinal waves were excited using a 0.5 MHz 25 mm diameter plane wave transducer (C0525-SB, Mana instruments).

The results at a snapshot in time are shown in Fig. 1 and the time evolution of the signals along the centre line of the substrates is shown in Fig. 4 (right). Snaps shots in time of the generation of the Lamb and Rayleigh wave modes waves are available in Appendix D. By tracing the lines of constant phase in Fig. 4 (right) the velocities of the excited waves can be estimated as $C_{A0} = 2625 \pm 50$ ms^{-1}, $C_R = 2962 \pm 50$ ms^{-1} and $C_{S0} = 5145 \pm 50$ ms^{-1} for the A0, Rayleigh and S0 devices respectively. These measured velocities are plotted on the dispersion curves shown in Fig. 2 and are in good agreement with the predicted velocities for the A0 (∘), Rayleigh (×) and S0 (+) modes for their respective substrates. These plots are also in good agreement with the simulations of the 3 mm substrate (Fig. 3) from which the mode shapes are derived matching the expected mode shapes for the A0 and S0 modes respectively. These fits are particularly good considering that the elastic constants for the printed material are not well characterised and frequently depend on the particularities of the print (see Section 4).

Fig. 4 (left) also shows the waves generated in the reverse direction and it can be seen that these are considerably smaller than those excited in the forward direction. This is in agreement with the design principles and the simulations shown in Fig. 3. The origin of the reverse waves is thought to primarily result from the reflections of the surface/plate modes created by the attachment of the pipes and this could be further reduced by apodizing the array [21] or changing the spacing to suppress the constructive interference from these sources [29].

6. Conversion efficiency

It is difficult to provide a definitive assessment of the energy conversion efficiency for these device experimentally because it is both hard to measure the energy input in the current experimental configuration accurately and because there are many interfaces between the transducer and the substrate which are hard to control in the experiment setup. The former problem originates because it is experimentally challenging to get an independent measurement of the field amplitude incident on the device in the current configuration despite it being possible to measure the absolute displacement amplitude on the substrate itself. The latter comes from the difficulty characterising the transducer-device and the device-substrate interfaces.

In order to estimate the conversion efficiency of the devices, additional modelling was performed (see Appendix E). The device was broken down into three separate models to isolate features that might contribute to losses and these were simulated on their own. The overall efficiency was then estimated by combining the losses at each stage. Consequently the first interface (bulk→pipes), the bend in the pipes, and the second interface (pipes→substrate) were simulated independently. The first interface caused small losses with transmission of $\sim 80\%$, the bend in the pipes caused negligible losses and the final interface had a transmission coefficient of $\sim 35-40\%$ depending on the specific device. The overall energy conversion efficiency for these devices was therefore estimated as $\sim 32\%$, $\sim 28\%$ $\sim 31\%$ for the A0, Rayleigh and S0 devices respectively. It is likely that the experimental conversion efficiency is lower because of the bond lines between the device and the transducer and the device and the substrate which were not included in the simulations. The losses result in reflections and mode conversions at the interfaces which results in reverberations — these can be observed experimentally in Fig. 4 as later arriving signals below/after the initial wave packets. It should be noted that these were simple proof-of-concept devices to demonstrate selective mode conversion and apart from adjusting the lengths of the pipes and ensuring normal incidence of the pipe to the substrate surface no attempt was made to optimise the energy conversion efficiency.

7. Concluding remarks

We have introduced a general method for coupling one elastic wave mode into another using an array of acoustic pipes to connect the modes and adjust the phase. We have demonstrated this for the conversion between longitudinal waves and various surface/plate modes. This technique is fairly general insofar as it is possible to couple a wide variety of wavemodes together provided a suitable structure linking them can be physically realised (see Fig. 3 and additional plots in Appendix A).

This is a new method of controlling elastic vibrations and may have many applications in a wide variety of areas where it is important to convert one elastic wave mode into another. It is worth noting that while the devices presented here are used to convert between two modes they could just as easily be used to arbitrarily shape the wavefront of the resulting wave and could therefore be used to steer, focus and create topological defects in the wavefields. This can be used to divert or harvest elastic wave energy [14,15,30,31] or enhance acoustic imaging [32–34]. This technique is generally applicable wherever it is possible to realise the topography required and may also inspire devices in photonics where similar devices (albeit at a different scale) may be used to control light. The use of this technique is widely applicable with potential to spark new paradigms of control and energy conversion across a wide range of wave regimes.

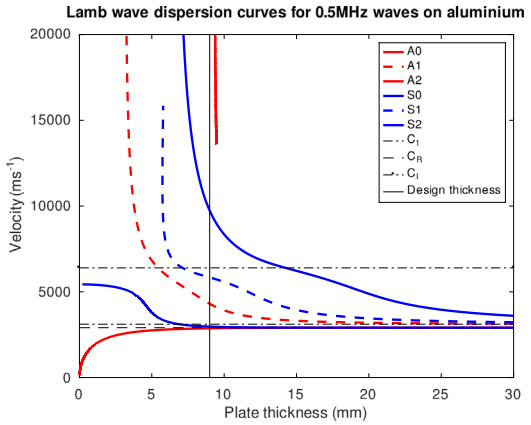

Fig. A.5. Extended version of the Lamb wave dispersion curves shown in Fig. 2. This shows a wider range of Lamb modes including A0, S0, A1, S1, A2 and S2 modes. The design point for the simulation shown in Fig. A.6 is indicated where the thickness equals 9 mm. It can be seen from the intersection of the curves with solid black line that the A0, S0, A1, S1 and S2 modes can be excited but the A2 mode cannot (as 0.5 MHz is below its cut-off frequency). It can also be seen that the A0 and S0 modes are nearly degenerate in phase velocity.

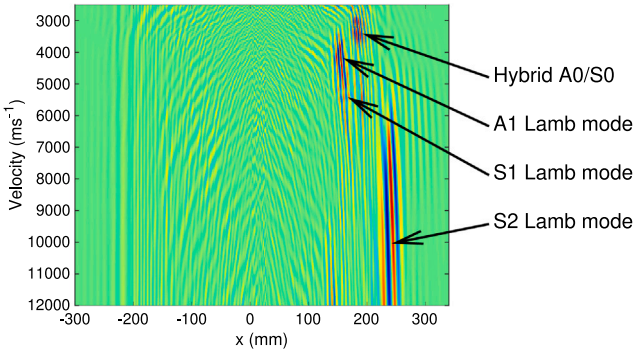

Fig. A.6. Extended simulation of devices showing a wider range of modes than evident in Fig. 3. In this simulation the substrate is kept at 9 mm thick and 16 acoustic pipes were used, otherwise the simulations were as for Fig. 3. These simulations are complex because it is difficult to find conditions where a simple sweep of the pipe lengths generates all the modes cleanly for illustration purposes. The number of fingers were increase to expand the footprint of the device on the substrate so long as to generate the longer wavelength/faster modes clearly. The modes labelled were identified by examining their phase velocity which was estimated from the wavelength of the disturbances observed.

CRediT authorship contribution statement

Rafael Fuentes-Domínguez: Conceptualization, Writing – review & editing. **Richard J. Smith:** Conceptualization, Writing – review & editing. **Peng Jin:** Investigation, Resources. **Marco Simonelli:** Investigation, Resources. **Samuel Gibbon:** Resources. **Matt Clark:** Writing – review & editing, Writing – original draft, Validation, Software, Resources, Methodology, Investigation, Funding acquisition, Formal analysis, Conceptualization.

Declaration of competing interest

The authors declare that they have no known competing financial interests or personal relationships that could have appeared to influence the work reported in this paper.

Acknowledgements

The authors would like to thank the support of the Engineering and Physical Sciences Research Council, UK through grants EP/K021877/1, EP/X000915/1, EP/V051814/1, EP/V029010/1, EP/S023275/1, EP/S013385/1 and EP/L022125/1.

Appendix A. Generation of a wider range of Rayleigh and Lamb modes

In order to demonstrate the possibility of generating a wider range of acoustic modes a revised model was simulated. This used a 9 mm thick substrate. It can be seen from Fig. A.5 that a 9 mm substrate supports A0, S0, A1, S1 and S2 Lamb modes at 0.5 MHz

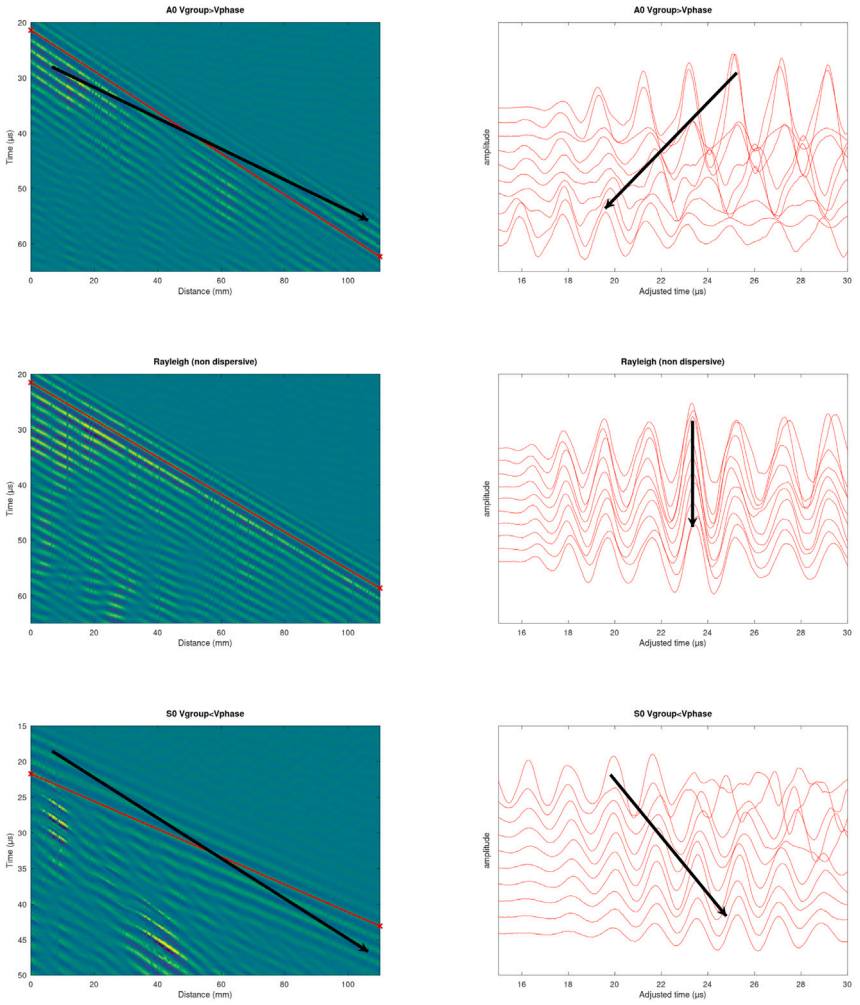

Fig. B.7. Plots of (left) amplitude vs time and distance. The red line shows a line of constant phase velocity and the black arrows in the A0 and S0 plots shows the shift in time of the wave packet determined by the group velocity. The Rayleigh wave is not dispersive and the wavepacket travels at the same speed as the phase velocity. (right) plots of wave amplitude vs adjusted time for 10 positions across the sample again black arrows show the shift of the wave packet due to any dispersion. Adjusted time involves subtracting $T_{adjust} = d/V_{phase}$ from the time axis on each plot, where d is the distance travelled. Here a non-dispersive wave will be seen to be stationary (as per the Rayleigh wave (right 2nd row)) where as the wavepacket moves left (shorter time) when $V_{group} > V_{phase}$ (A0 mode, top) and right when $V_{group} < V_{phase}$ (S0 mode bottom). (For interpretation of the references to colour in this figure legend, the reader is referred to the web version of this article.)

(but not A2 or any higher order modes). The model was set up as per Appendix E and run sweeping the design frequency from 2500 to 12 000 ms^{-1}. The modes generated were then identified and labelled according to their phase velocity which was measured by estimating the wavelength from the simulations.

Appendix B. Additional analysis of the group velocity

Fig. 4 in the main text shows the time-space response of the generated waves on the substrate. On close examination it is apparent that both the A0 and S0 modes are dispersive because the group velocity is not equal to the phase velocity. In order to make this clearer, details of these plots with the group velocity shift highlighted by arrows together with adjusted time plots for ten positions are shown in Fig. B.7.

Appendix C. Detailed design drawings

In this appendix detailed scale drawings of the devices from the side are shown in Fig. C.8 and for reference purposes the lengths of the acoustic pipes are tabulated in Table C.1. The excess length for each successive pipe is given by $\delta d_{pipe} = \delta x C_{plate}/C_{pipe}$ as described in Section 2 and Fig. 2 in the main text and in Fig. E.10 in Appendix E.

Fig. C.8. Detailed scale illustration of the three devices used in the paper for A0, Rayleigh and S0 conversion left–right. The pipe and gap size is 1 mm each at both ends. In order to keep a similar compact size for all three devices the angle at which the body wave was incident was 90 degrees for the A0 and Rayleigh devices and 45 degrees for the S0 device. Provided the pipes are not required to bend too sharply this is an arbitrary parameter (see Appendix E.2) and arbitrary angles can be accommodate provided the pipes are long enough to accommodate the extra phase matching length required without requiring a too-tight bend radius.

Table C.1
Table detailing the lengths around the pipe for each device shown in Fig. C.8. In each case the pipe is 1 mm thick and the spacing is 1 mm.

Pipe #	A0 length (mm)	Rayleigh length (mm)	S0 length (mm)
1	29.45	29.45	29.45
2	33.72	33.20	31.56
3	37.99	36.94	33.66
4	42.26	40.68	35.76
5	46.53	44.42	37.87
6	50.80	48.17	39.97
7	55.56	51.91	42.07
8	59.33	55.65	44.17
9	63.60	59.39	46.28
10	67.87	63.14	48.38

Appendix D. Additional simulations of conversion with snap shots in time

To assist with the understanding of the conversion process, the final model from Appendix E.3 was used to generate multiple snapshots in time. The start time is set to $T = 0$ when the wave first becomes visible in the picture and then snapshots are shown every 5 μs until 70 μs when the generated Lamb or Rayleigh wave is fully in the substrate. It can be seen in Fig. D.9 that the waves in the pipes arrive with various delays. These delays time the arrival of the S0 mode in the pipe with the moving wave in the substrate to constructively add to the wave amplitude of the desired mode moving in the desired direction. In these simulations, the reflections from the boundaries are not seen because the pipes are of sufficient length that they do not re-enter the frame within the simulation times shown.

Appendix E. Assessment of conversion efficiency

Assessing energy conversion efficiency is a complex task. As discussed in Section 6 this is currently difficult to measure experimentally because it is difficult to (a) measure the displacement field at the input to the device and (b) difficult to account for the interfaces between the various components. In order to provide an assessment of the conversion efficiency we have broken the problem down into three parts: (1) the conversion of the longitudinal wave incident on surface S_s (Fig. 2 and reproduced here in Fig. E.10) into S0 plate modes in the acoustic pipes, (2) transmission of the energy around the curve of the pipes from S_s to S_d and (3) conversion of the S0 modes in the pipes to the required Rayleigh/Lamb mode in the substrate. Each of these can be modelled efficiently in isolation without the complications of additional interfaces, reflections or reverberations. It should also be noted that the devices presented here are simply proof-of-concept designs intended to demonstrate selective mode conversion and no attempt was made to enhance the conversion efficiency or reduce losses due to reflections at the various boundaries.

In each of these simulations the geometry was altered so that the initial disturbance could enter the entire structure before the interface (or bend) and then fully exit without encountering another interface. Consequently the total strain energy for the incident and transmitted modes could be evaluated by integrating the strain energy over the appropriate region (at an appropriate time) and, consequently, the energy transmission efficiency for that part of the structure could be estimated in isolation from all other interfaces.

The total energy efficiency of the complete structure can then be computed by combining the three stages. Because this allows any reflections to be spatially and temporally isolated it avoids any problems where there might be overlap of reflected waves or additional modes and gives a reasonable estimate of the total efficiency.

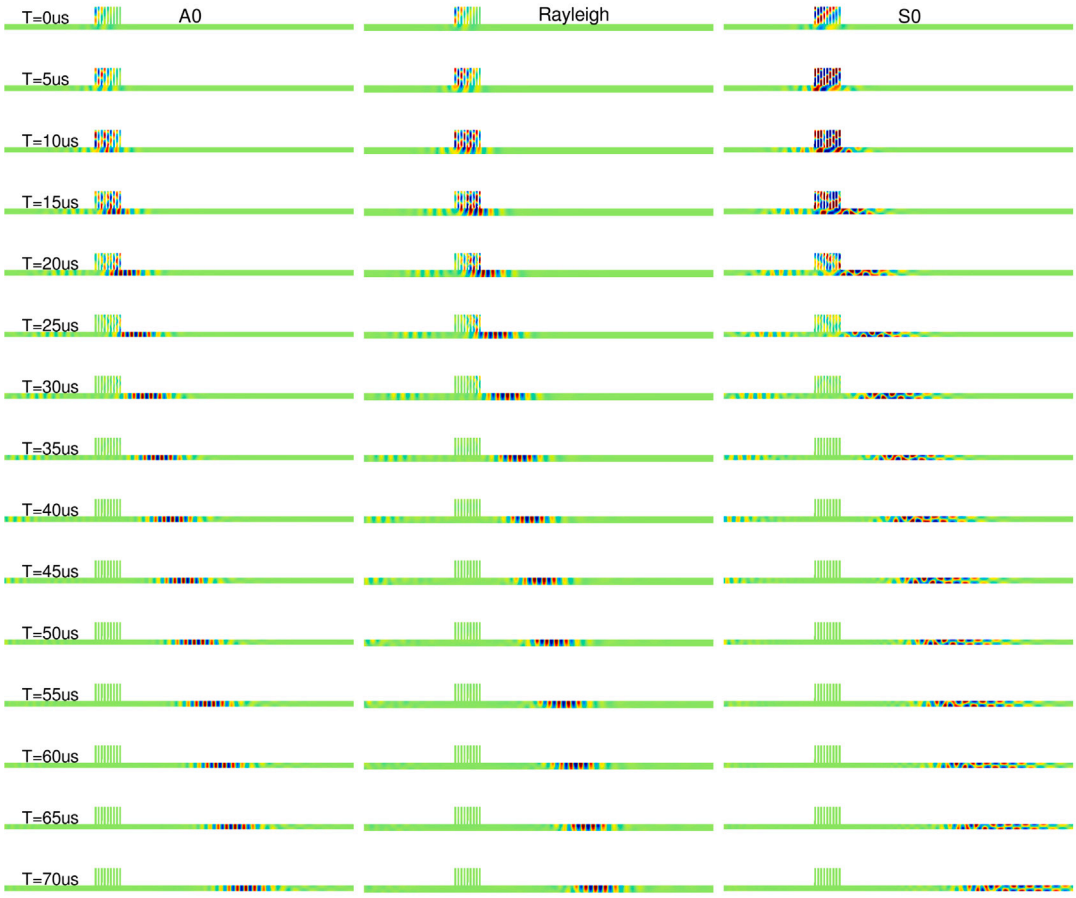

Fig. D.9. Time shots of the conversion. In these models the conversion process to the A0, Rayleigh and S0 modes is displayed at many time snapshots. The full length of the acoustic pipes and the full thickness of the Rayleigh wave substrate have been truncated for illustrative purposes.

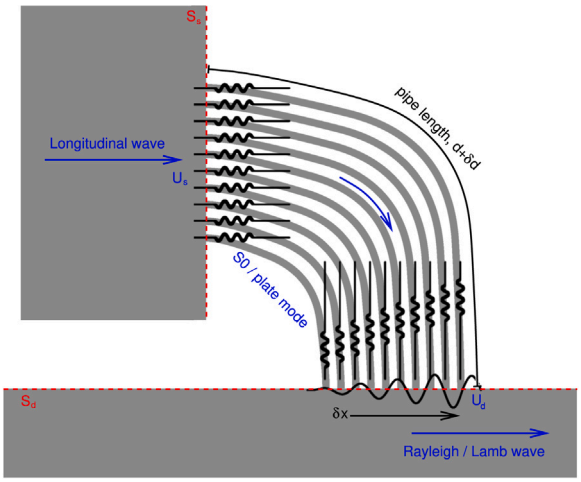

Fig. E.10. Schematic of the device and its mode of operation reproduced from Fig. 2 in the body text. The incident longitudinal wave enters the device and is divided amongst the ‘‘acoustic pipes’’ which act as waveguides.

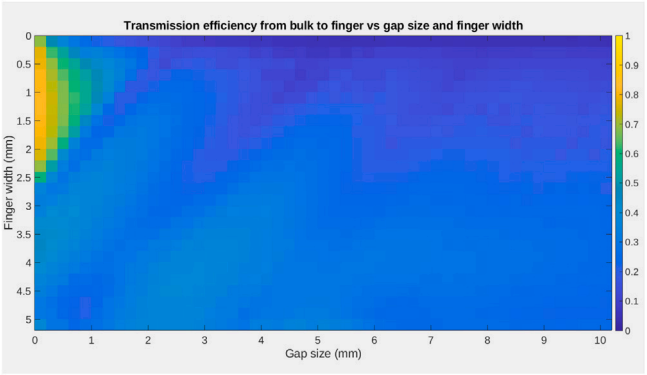

Fig. E.11. Transmission coefficient for the bulk→S0/plate mode conversion at the interface between the solid body and array of acoustic pipes vs the width of the pipes and the gap spacing between them. It can be observed that there is an area of high transmission coefficient (top left) where the pipes are narrow and the gaps are small. This is regime where the devices presented in this paper operate (these devices have a transmission efficiency of 0.8). This region is bounded by a dip in transmission along a 45 degree band corresponding to a period (gap + width) ∼ 6 mm. This band is repeated roughly at even intervals where the period (gap + width) ∼ $n \times 6$ mm, where n is an integer. These dips were found to be due to a resonant transverse mode confined to the region between the pipes and corresponds to a standing wave mode with approximately the velocity of the Rayleigh or shear mode. This gives rise to an enhanced reflection coefficient at these periods and a reduced transmission coefficient. For these pipe widths the only mode that can be excited is the S0 since the A0 and A1 modes cannot be excited by symmetry and the width is below the cut-off for the S0 mode (see Fig. 2 in the main paper).

E.1. Conversion from longitudinal to S0/plate modes at surface S_s

In order to model the conversion between the longitudinal mode and the S0/plate mode in the acoustic pipes a model was set up consisting of a solid block with an acoustic pipe projecting from it. The complete model was made by using periodic boundary conditions to repeat the block infinitely and it was parameterised for the width of the acoustic pipe and the gap spacing between them. These two parameters where then scanned from much smaller to much larger values than the ones the device used. The length of the solid block and the pipe was chosen such that the complete wave train would fit in either before and after transmission. The elastic strain energy was evaluated at two points in time, first when the complete wave packet was in the block and secondly when the complete wave packet was in the pipe. The transmission coefficient as a function of pipe width and gap size is shown in Fig. E.11.

A series of dips in the transmission coefficient can be observed as diagonal lines across the plot in Fig. E.11. These are due to the effect of a standing transverse mode (confined to the interface region). This is a resonant effect that occurs when the period of the structure (gap + width) corresponds to the period of the surface/shear mode across the surface.

The devices presented in this paper occupy the high transmission region in Fig. E.11 in the upper left region of the plot corresponding to an energy transmission coefficient of ∼ 0.8. This could be improved simply by decreasing the gap size between the pipes. This was trivially set at 1 mm for the devices demonstrated here to facilitate easy powder removal during manufacture.

E.2. Transmission of energy from end-to-end of the acoustic pipes around a bend radius

Fig. E.12 shows the transmission coefficient of the curved acoustic pipe in isolation. The model consists of a straight section joined to a curve of constant radius joined to a straight section with no variation in thickness. The total strain energy in the initial straight section at an early time when the complete wave packet completely contained in this initial straight section is used to measure the input energy. The total strain energy at a later time when the transmitted S0 wavepacket is in the second straight section is used to measure the transmission. It was observed that for tight bending radii additional modes were excited around the bend, by virtue of the timing points used these were easily separated by the spatially filtering the S0 mode.

For all the bend radii and angles used in this paper the transmission coefficient for the pipes can be seen to be $\simeq 1$ and will be taken to be unity for the purposes of efficiency estimates.

E.3. Conversion from S0/plate mode in the acoustic pipes to Rayleigh/Lamb mode in the substrate at surface S_d

In order to estimate the efficiency of conversion from the acoustic pipes a model was constructed with straight pipes connected to the surface with lengths to give the appropriate timings for the desired substrate mode and the wave packets was excited at the end of the pipe. The pipes were of sufficient length that the complete wave packet could be completely contained within the pipes at one moment in time and the total input strain energy was computed at this point. The model was then run until the desired mode was propagating fully in the substrate (see Fig. D.9). At this point it was possible to spatially isolate it from other disturbances and the total strain energy was computed in this region at this point in time. From this it was possible to estimate the conversion from the pipes to the A0, Rayleigh and S0 modes as ∼ 39%, ∼ 35% and ∼ 38% respectively.

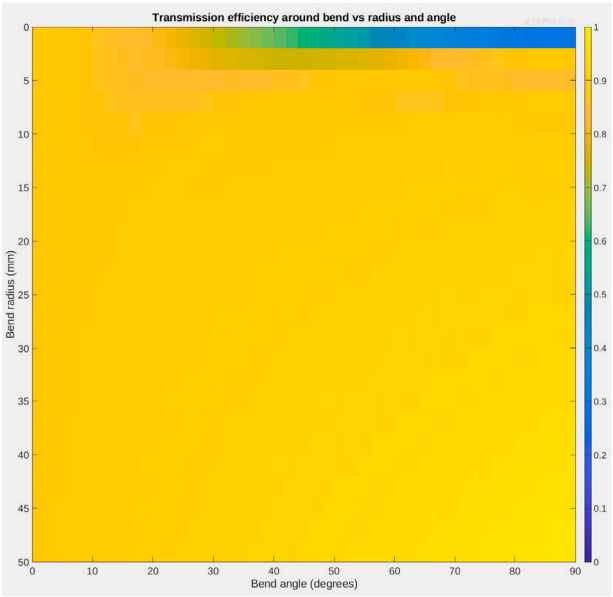

Fig. E.12. Transmission coefficient for the S0/plate mode through the acoustic pipes as a function of bend radius and bend angle. It can be seen that for bend radii>wavelength (~ 11 mm) the transmission is $\simeq 1$. At tight bend radii and larger bend angles the behaviour is complex due to resonant behaviour around the tight bend radii and the excitation of additional modes (see [2]).

E.4. Total efficiency and discussion

By combining the efficiency of conversion at each stage the overall energy conversion efficiency can be estimated as $\sim 32\%$, $\sim 28\%$ $\sim 31\%$ for the A0, Rayleigh and S0 devices respectively. It should be noted that, apart from the adjustment of the pipe lengths to match the phase condition and the choice of normal angle of incidence, no attempt was made to optimise the structures for transmission efficiency. The remaining energy was observed to be reflected back through the acoustic pipes which then reverberated through the system giving rise to the later time signals that can be observed in Fig. 4 in the main paper. Since these reverberations will become dephased by multiple round trips in the pipes they can also be observed to excite additional modes at these later times especially in the S0 plot in Fig. 4. It is also likely that the experimental efficiency of the devices is lower than the estimate from the models as there are additional interfaces such as the transducer→device bond line and device→substrate bond line which were not included in the simulations.

Data availability

Data will be made available on request.

References

[1] K.F. Graff, Wave Motion in Elastic Solids, Oxford University Press, 1975.
[2] I.A. Viktorov, Rayleigh and Lamb Waves, Plenum Press, 1967.
[3] G.J. Chaplain, J.M. De Ponti, A. Colombi, R. Fuentes-Dominguez, P. Dryburg, D. Pieris, R.J. Smith, A. Clare, M. Clark, V.R. Craster, Tailored elastic surface to body wave umklapp conversion, Nat. Commun. 11 (1) (2020) http://dx.doi.org/10.1038/s41467-020-17021-x.
[4] R. Fuentes-Domínguez, M. Yao, A. Colombi, P. Dryburgh, D. Pieris, A. Jackson-Crisp, D. Colquitt, A. Clare, R.J. Smith, M. Clark, Design of a resonant luneburg lens for surface acoustic waves, Ultrasonics 111 (2021) 106306.
[5] K.L. Tsakmakidis, A.D. Boardman, O. Hess, 'Trapped rainbow' storage of light in metamaterials, Nature 450 (7168) (2007) 397–401.
[6] J. Zhu, Y. Chen, X. Zhu, F.J. Garcia-Vidal, X. Yin, W. Zhang, X. Zhang, Acoustic rainbow trapping, Sci. Rep. 3 (2013) 1728 EP.
[7] M. Clark, Two-dimensional, three-dimensional, and gray-scale images reconstructed from computer-generated holograms designed by use of a direct-search method, Appl. Opt. 38 (25) (1999) 5331–5337.
[8] M. Redwood, Mechanical Waveguides : The Propagation of Acoustic and Ultrasonic Waves in Fluids and Solids with Boundaries, Pergamon Press, 1960.
[9] R. Singh, A. Gupta, O. Tripathi, S. Srivastava, B. Singh, A. Awasthi, S. Rajput, P. Sonia, P. Singhal, K.K. Saxena, Powder bed fusion process in additive manufacturing: An overview, Mater. Today: Proc. 26 (2020) 3058–3070.
[10] L.Y. Yeo, J.R. Friend, Surface acoustic wave microfluidics, Annu. Rev. Fluid Mech. 46 (1) (2014) 379–406.
[11] A. Briggs, Acoustic Microscopy, Clarendon Press, 1992.
[12] P. Dryburgh, W. Li, D. Pieris, R. Fuentes-Domínguez, R. Patel, R.J. Smith, M. Clark, Measurement of the single crystal elasticity matrix of polycrystalline materials, Acta Mater. 225 (2022) 117551.
[13] F.A. Dahlen, J. Tromp, Theoretical Global Seismology, Princeton University Press, Princeton, New Jersey, 1998.

[14] A. Colombi, D. Colquitt, P. Roux, S. Guenneau, R.V. Craster, A seismic metamaterial: The resonant metawedge, Sceintific Rep. 6 (2016) http://dx.doi.org/10.1038/srep27717.
[15] Y. fan Liu, J. kun Huang, Y. guang Li, Z. fei Shi, Trees as large-scale natural metamaterials for low-frequency vibration reduction, Constr. Build. Mater. 199 (2019) 737–745.
[16] D. Cardella, P. Celli, S. Gonella, Manipulating waves by distilling frequencies: a tunable shunt-enabled rainbow trap, Smart Mater. Struct. 25 (2016) (8):085017.
[17] J.M. De Ponti, A. Colombi, R. Ardito, F. Braghin, A. Corigliano, R.V. Craster, Graded elastic metasurface for enhanced energy harvesting, New J. Phys. (2019).
[18] S. Alan, A. Allam, A. Erturk, Programmable mode conversion and bandgap formation for surface acoustic waves using piezoelectric metamaterials, Appl. Phys. Lett. 115 (9) (2019).
[19] R. White, Surface elastic waves, Proc. IEEE 58 (8) (1970) 1238–1276, http://dx.doi.org/10.1109/PROC.1970.7900.
[20] R.M. White, F.W. Voltmer, Direct piezoelectric coupling to surface elastic waves, Appl. Phys. Lett. 7 (12) (2004) 314–316.
[21] D. Malocha, Surface acoustic wave design fundamentals, Arch. Acoust. 21 (4) (2014) 387–398.
[22] V.V. Krylov, Generation of ground vibrations by superfast trains, Appl. Acoust. 44 (2) (1995) 149–164, http://dx.doi.org/10.1016/0003-682X(95)91370-I.
[23] COMSOL Multiphysics, COMSOL AB, 2019, URL https://www.comsol.com.
[24] P.L. Marston, Negative group velocity lamb waves on plates and applications to the scattering of sound by shells, J. Acoust. Soc. Am. 113 (5) (2003) 2659–2662.
[25] OpenSCAD, openscad.org, 2024, URL https://openscad.org.
[26] MATLAB, The MathWorks Inc., 2024, URL https://www.mathworks.com.
[27] J.W. Eaton, D. Bateman, S. Hauberg, R. Wehbring, GNU octave, 2023, URL https://www.gnu.org/software/octave/.
[28] E.M. Sefene, State-of-the-art of selective laser melting process: A comprehensive review, J. Manuf. Syst. 63 (2022) 250–274, http://dx.doi.org/10.1016/j.jmsy.2022.04.002.
[29] M. Clark, F. Linnane, S.D. Sharples, M.G. Somekh, Frequency control in laser ultrasound with computer generated holography, APL 72 (16) (1998) 1963–1965.
[30] G. Lee, S.-J. Lee, J. Rho, M. Kim, Acoustic and mechanical metamaterials for energy harvesting and self-powered sensing applications, Mater. Today Energy 37 (2023) 101387.
[31] H.-W. Dong, S.-D. Zhao, P. Xiang, B. Wang, C. Zhang, L. Cheng, Y.-S. Wang, D. Fang, Porous-solid metaconverters for broadband underwater sound absorption and insulation, Phys.Rev. Appl. 19 (2023) 044074, http://dx.doi.org/10.1103/PhysRevApplied.19.044074.
[32] Q. Lu, X. Li, X. Zhang, M. Lu, Y. Chen, Perspective: Acoustic metamaterials in future engineering, Engineering 17 (2022) 22–30.
[33] Z. Li, D.-Q. Yang, S.-L. Liu, S.-Y. Yu, M.-H. Lu, J. Zhu, S.-T. Zhang, M.-W. Zhu, X.-S. Guo, H.-D. Wu, X.-L. Wang, Y.-F. Chen, Broadband gradient impedance matching using an acoustic metamaterial for ultrasonic transducers, Sci. Rep. 7 (1) (2017) 42863.
[34] G. Liao, C. Luan, Z. Wang, J. Liu, X. Yao, J. Fu, Acoustic metamaterials: A review of theories, structures, fabrication approaches, and applications, Adv. Mater. Technol. 6 (5) (2021) 2000787.